Journal of the Korean Physical Society, Vol. 30, No. 1, February 1997, pp. 123∼130

High Quantum-Efficiency 4H-SiC UV Photodiode

Kook-Sang Park

Department of Physics, Kongju National University, Chungnam 314-701

Tsunenobu Kimoto and Hiroyuki Matsunami

Department of Electrical Engineering, Kyoto University, Yoshidahonmachi, Sakyo, Kyoto 606, Japan

(Received 9 May 1996, in final form 30 December 1996)

We have designed a 4H-SiC UV photodiode having a $n^+/p/p$ structure sensitive to ultraviolet radiation. The quantum efficiency of the photodiode was calculated by properly choosing parameters to increase the ultraviolet photoresponse. The wavelength at which the peak response occurred could be well controlled by varying the junction depth, the geometric structure of the photodiode, the doping concentrations of the n- and the p-layers, and the thickness of the anti-reflective layer. We expect a good photoresponse in this 4H-SiC homostructure for the wavelength range of 200∼380 nm. The highest internal quantum efficiency of the 4H-SiC photodiode came to about 92% for a peak at 257 nm. Also, the calculated external quantum-efficiency curve of the 4H-SiC photodiode shifted to shorter UV wavelength compared with the calculated one for 6H-SiC photodiode with nearly the same parameters. In addition, the peak of the external quantum efficiency of the 4H-SiC photodiode (about 90% at 257 nm) was higher by about 5% than that of a 6H-SiC photodiode (about 85% at 270 nm).

I. INTRODUCTION

Silicon carbide (SiC) has been applied in optoelectronic devices for the detection of ultraviolet (UV) radiation and for the generation of blue light. SiC has high optical absorption in the UV range and sufficient diffusion length for the collection of generated charge carriers. As the wide-bandgap of SiC leads to a very low level of the diode dark current, it may be also used in high-temperature environments. SiC photodiodes have many applications such as detecting UV radiation from rocket plumes for combustion control, UV monitoring for industrial processes and UV curing, and sun-exposure monitoring using a personal UV detector. Analysis applications include air-quality monitoring equipment and UV spectroscopy [1].

As a reported result, 6H-SiC photodiodes were made by Brown *et al.* [2]. However, it is well known that the physical properties of the hexagonal 4H-SiC polytype are more attractive than those of 6H-SiC for advanced device application. 4H-SiC has a sufficiently large bandgap (3.26 eV at 300 K) and the highest electron mobility among hexagonal SiCs. 4H-SiC single crystals have been controllably grown by a modified Lely method. Moreover, high-quality 4H-SiC epitaxial growth has been achieved by step-controlled chemical vapor deposition (CVD) [3]. The control of the conduction types (n- or p-type) and the carrier concentrations is possible by in-situ doping. Since the epitaxial growth of 4H-SiC has reached an acceptable level for device fabrication, the research on and the development of devices utilizing 4H-SiC should accelerate rapidly. 4H-SiC is currently perceived as a potential material superior to 6H-SiC for high-power, high-frequency, and high-temperature electronic devices. In addition, there is no doubt that the UV photoresponse of 4H-SiC will be much superior to that of 6H-SiC by virtue of the higher mobilities and the longer diffusion lengths of 4H-SiC.

Brown's diffusion model of the generated carriers for the calculation of the quantum efficiency does not contain the effect of the depletion region, as can be seen in their boundary conditions for the calculation of the quantum efficiency, and the Einstein relation and the definition relation of the diffusion length are neglected entirely. However, the width of the depletion region and the relations between the parameters should be considered whenever the quantum efficiency of a photodiode is calculated. The purpose of this paper is to design a 4H-SiC UV photodiode that can detect UV radiations at shorter wavelengths with a high photoresponse. Another purpose is to show the effective contribution of the depletion region to the quantum efficiency, which has not considered in the case of SiC photodiodes. Then, the parameters of the photodiode should be connected by equations such as the Einstein relation and the defini-

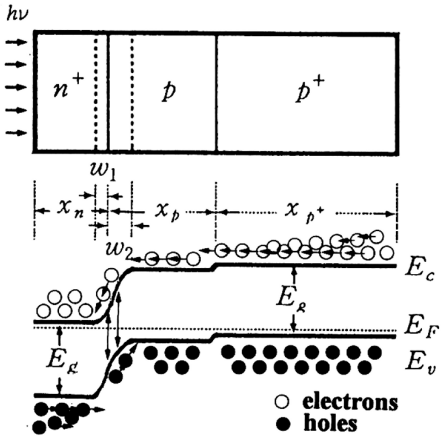

Fig. 1. The diffusion model of the minority carriers and the energy-band diagram of the 4H-SiC photodiode.

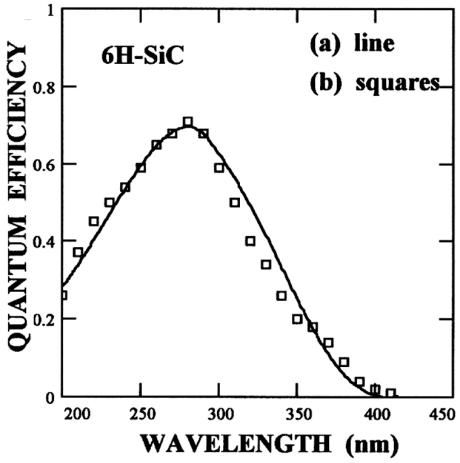

Fig. 2. The quantum efficiency of a 6H-SiC photodiode (device #1): (a) the calculated and (b) the measured quantum efficiency [2].

tion of the diffusion length which is related to the carrier lifetime.

The parameters in this study were properly adjusted to obtain high photoresponse. We calculated the quantum efficiency of the 4H-SiC photodiode by properly choosing the parameters to enhance the UV photoresponse. The main parameters were the doping concentration, the mobility and the lifetime of the carriers, the geometric structure of the photodiode, and the thickness of the anti-reflective layer. We demonstrate the variation of the quantum efficiency as a function of the wavelength for different parameters in the one-dimensional model about the diffusion of the minority carriers. In this model, the effect of the depletion region at the n^+/p junction is included, and it appears to contribute significantly to the quantum efficiency. Finally, the parameters were chosen to increase the quantum efficiency of the 4H-SiC photodiode, and the calculated result was compared with the measured one for 6H-SiC [2].

II. A DIFFUSION MODEL OF THE MINORITY CARRIERS

Figure 1 shows the diffusion model of the minority carriers and the energy-band diagram of a 4H-SiC photodiode having $n^+/p/p$ structure that were used for the calculation of the quantum efficiency. This model includes transmission of light through an overlying SiO_2 anti-reflective layer, the photon absorption within each layer of 4H-SiC, and the collection of charges generated by photon absorption. It is possible to find analytical expressions for the quantum efficiency under cer-

Table 1. 4H-SiC parameters of the minority carriers for the calculation of the quantum efficiency at 300 K [9–11].

n-layer	N_d (cm^{-3})	μ_p (cm^2/Vs)	τ_p (ns)	D_p (cm^2/s)	L_p (cm)
6H-SiC	5×10^{18}	40	10	1.04	1.0×10^{-4}
4H-SiC	5×10^{18}	50	10	1.30	1.2×10^{-4}
p-layer	N_a (cm^{-3})	μ_n (cm^2/Vs)	τ_n (ns)	D_n (cm^2/s)	L_n (cm)
6H-SiC	5×10^{17}	60	20	1.55	1.8×10^{-4}
6H-SiC	5×10^{15}	120	20	3.10	2.5×10^{-4}
4H-SiC	5×10^{17}	80	20	2.07	2.0×10^{-4}
4H-SiC	5×10^{16}	100	20	2.28	2.6×10^{-4}
4H-SiC	5×10^{15}	150	20	3.88	2.8×10^{-4}

Table 2. Typical device structure for the calculation of the quantum efficiency: (a) concentrations(cm^{-3}) and (b) thicknesses(μm) in each layer.

Device No.		n^+-layer	p-layer	p-substrate	SiO_2
* 6H-SiC	(a)	5×10^{18}	5×10^{17}	5×10^{17}	
#1	(b)	0.05	5.0		0.055
4H-SiC	(a)	5×10^{18}	5×10^{16}	5×10^{17}	
#2	(b)	0.1	3.0	200	—
6H-SiC	(a)	5×10^{18}	5×10^{15}	5×10^{17}	
#3	(b)	0.05	3.0	200	0.055
4H-SiC	(a)	5×10^{18}	5×10^{15}	5×10^{17}	
#4	(b)	0.05	3.0	200	0.045

∗ Ref. 1

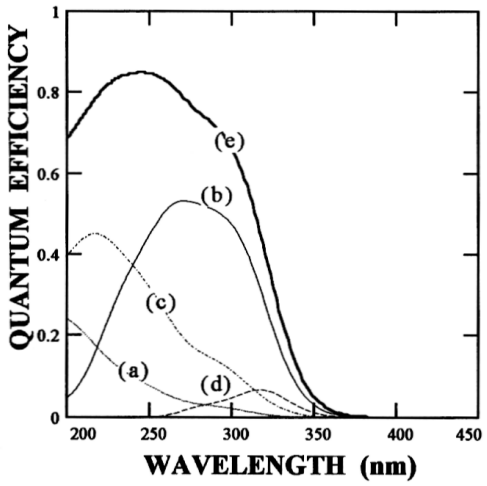

Fig. 3. The total quantum efficiency and the individual contributions to the quantum efficiency in each layer (device #2): (a) n^+-layer, (b) p-layer, (c) depletion region, (d) substrate, and (e) total quantum efficiency.

tain idealized conditions neglecting the series- and shunt-resistance losses.

From Lambert's law of optical absorption, the number of photons absorbed per unit time in unit area of a layer of thickness dx at a distance x below the surface is given by [4]

$$g(x)dx = \alpha(\lambda)N(\lambda)\{\ 1 - R(\lambda)\}\ e^{-\alpha(\lambda)\ x}dx \qquad (1)$$

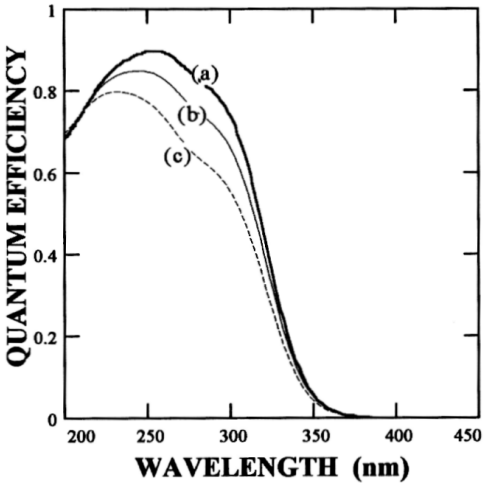

Fig. 5. The quantum efficiency for different acceptor concentrations (N_a) in the p-layer (device #2): (a) 5×10^{15} cm^{-3}, (b) 5×10^{16} cm^{-3}, and 5×10^{17} cm^{-3}.

where $\alpha(\lambda)$ is the optical absorption coefficient at a wavelength λ, $N(\lambda)$ the number of incident photons per cm^2/s per unit bandwidth, and $R(\lambda)$ the reflectivity from the surface.

For a steady-state condition, the continuity equation for the holes in the n^+-layer in the absence of an electric field is [5]

$$\frac{d^2p(x)}{dx^2} - \frac{p(x)}{L_p^2} = -\frac{\alpha(\lambda)}{D_p}N(\lambda)\{\ 1 - R(\lambda)\}\ e^{-\alpha(\lambda)\ x} \qquad (2)$$

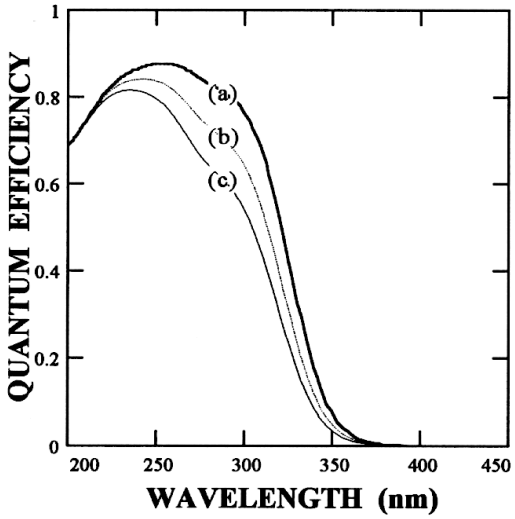

Fig. 4. The quantum efficiency for different electron lifetimes in the p-layer (device #2): (a) 50 ns, (b) 20 ns, and (c) 10 ns.

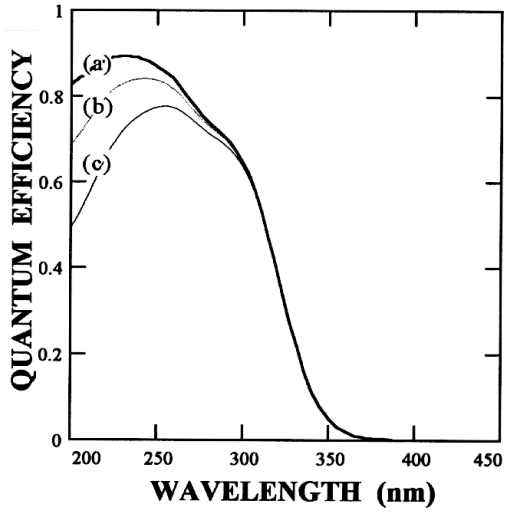

Fig. 6. The quantum efficiency for different thicknesses of the n^+-layer (device #2): (a) 0.05 μm, (b) 0.1 μm, and (c) 0.2 μm.

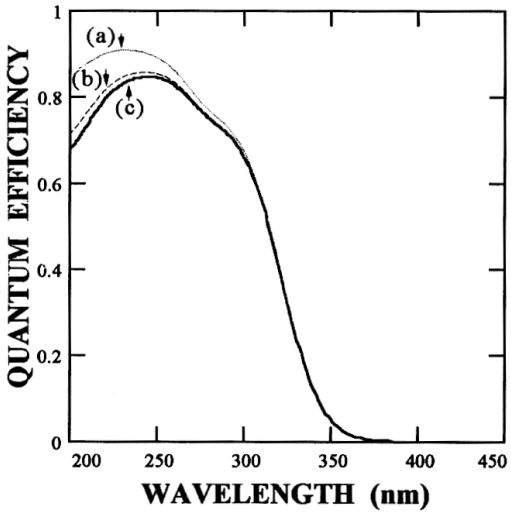

Fig. 7. The variation of the quantum efficiency for different surface recombination velocities in the n^+-layer (device #2): (a) 1.0×10^5 cm/s, (b) 1.0×10^6 cm/s, and (c) 3.0×10^7 cm/s.

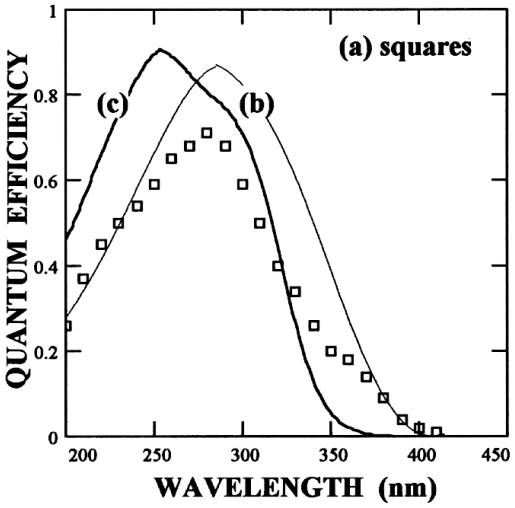

Fig. 9. The external quantum efficiency of the 4H-SiC photodiode compared with that of the 6H-SiC photodiode: (a) the measured quantum efficiency (device #1) [2], (b) the calculated quantum efficiency of a 6H-SiC photodiode (device #3), and (c) the calculated quantum efficiency of a 4H-SiC photodiode (device #4).

where $p(x)$ is the excess concentration at a distance x in the n^+-layer, L_p the diffusion length for the holes, and D_p the diffusion coefficient for the holes. The general solution of this inhomogeneous differential equation for the holes in n^+-type materials is given by

$$p(x) = A_p \cosh\left(\frac{x}{L_p}\right) + B_p \sinh\left(\frac{x}{L_p}\right) - \frac{\alpha(\lambda)N(\lambda)\{\,1-R(\lambda)\}\,\tau_p}{\{\,\alpha(\lambda)^2L_p^2-1\}} e^{-\alpha(\lambda)\,x}, \quad (3)$$

and the general solution of the equivalent equation for the electrons in p-type materials is given by

$$n(x) = A_n \cosh\left(\frac{x}{L_n}\right) + B_n \sinh\left(\frac{x}{L_n}\right) - \frac{\alpha(\lambda)N(\lambda)\{\,1-R(\lambda)\}\,\tau_n}{\{\,\alpha(\lambda)^2L_n^2-1\}} e^{-\alpha(\lambda)\,x} \quad (4)$$

where $n(x)$ is the excess concentration at a distance x in the p-layer, L_n the diffusion length for the electrons, and τ_p and τ_n the lifetimes of the holes and the electrons, respectively. The constants A_p, B_p, A_n, and B_n

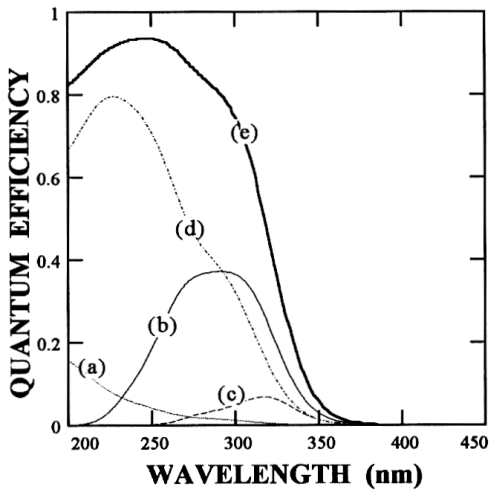

Fig. 8. The total internal quantum efficiency and the individual contributions to the quantum efficiency in each layer (device #4, except for SiO_2): (a) n^+-layer, (b) p-layer, (c) substrate, (d) depletion region, and (e) total quantum efficiency.

Table 3. Anisotropy of the calculated effective masses of 6H-SiC and 4H-SiC, and those of 4H-SiC obtained experimentally from IR-absorption measurement [13–16].

Polytype	m_n/m_o(‖c-axis)	m_n/m_o(⊥ c-axis)
6H-SiC (cal.)	0.13	0.35
4H-SiC (cal.)	0.19	0.21
4H-SiC (exp.)	0.18	0.22

(cal.): Calculated values
(exp.): Experimentally obtained values

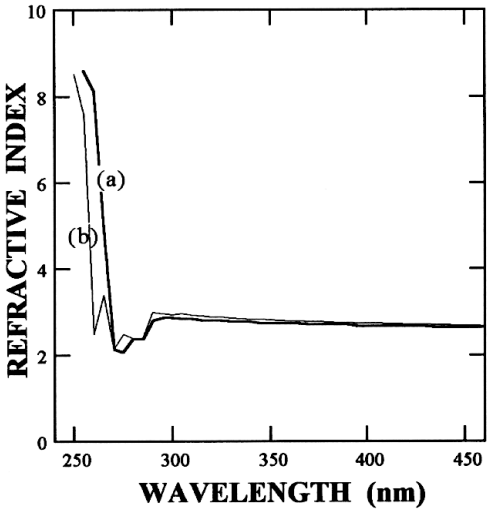

Fig. 10. The refractive indices of (a) 6H-SiC and (b) 4H-SiC as a function of wavelength.

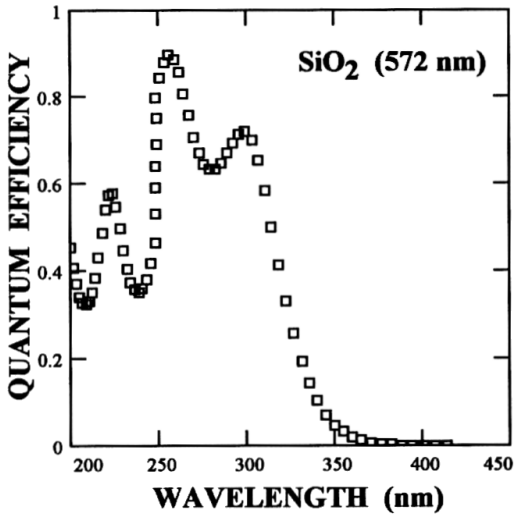

Fig. 11. The external quantum efficiency for a SiO_2 thickness of 572 nm with the other parameters of device #4.

in Eqs. (3) and (4) can be determined by the boundary conditions imposed by the device structure and the parameters. The boundary conditions are given by [7]

$$D_p \left[\frac{dp(x)}{dx}\right]_{x=0} = S_p\, p_n(0), \tag{5}$$

$$p(x_n - w_1) = n(x_p - w_2) = 0, \tag{6}$$

$$n(x_n + x_p) = n^+(x_n + x_p), \tag{7}$$

$$D_n \left[\frac{dn(x)}{dx}\right]_{x=x_n+x_p} = D_{n^+}\left[\frac{dn^+(x)}{dx}\right]_{x=x_n+x_p}, \tag{8}$$

and

$$-D_n \left[\frac{dn^+(x)}{dx}\right]_{x=x_{p^+}} = S_n n^+(x_{p^+}) \tag{9}$$

where S_p and S_n are the surface recombination velocities for the holes and the electrons, respectively, and x_n, x_p, and x_{p^+} the thicknesses of the n^+-layer, the p-layer, and the p-substrate, respectively. An ohmic contact is applied to the back-surface so that in these cases $S_n \to \infty$. We solve Eqs. (3) and (4) by applying the above boundary conditions for $p(x)$ and $n(x)$. The current densities $J(\lambda)$ in the n^+/p junction are then determined by the minority carrier gradients on both sides of the junction and the depletion layer. Besides, the internal quantum efficiency $\eta(\lambda)$ of the photodiode is defined as the number of electron-hole pairs collected under short circuit conditions relative to the number of photons entering the photodiode, that is [5],

$$\eta(\lambda) = \frac{J(\lambda)}{qN(\lambda)\{\,1 - R(\lambda)\}} \tag{10}$$

where $J(\lambda)$ is the photocurrent density as a function of wavelength λ, and q the electronic charge. The quantum efficiency component η_p to get the hole contribution in the n^+-layer is [2,6,7]

$$\eta_p(\lambda) = \frac{\alpha L_p}{\alpha^2 L_p^2 - 1}\left[\frac{S_p + \alpha D_p - e^{\{\,-\alpha(x_n - w_1)\}}\,\{S_p \cosh(\frac{x_n - w_1}{L_p}) + \frac{D_p}{L_p}\sinh(\frac{x_n - w_1}{L_p})\}}{\frac{D_p}{L_p}\cosh(\frac{x_n - w_1}{L_p}) + S_p \sinh(\frac{x_n - w_1}{L_p})} - \alpha L_p e^{\{\,-\alpha(x_n - w_1)\}}\right] \tag{11}$$

where w_1 and w_2 are the widths of the depletion layer extended to the n^+- and the p-layer sides, respectively. Now, we compute the quantum efficiency component η_n to get the electron contribution in the p-layer and to get η_{n^+} in the p-substrate:

$$\eta_n(\lambda) = \frac{\alpha L_n e^{\{\,-\alpha(x_n + w_2)\}}}{\alpha^2 L_n^2 - 1}\left[\alpha L_n - \tanh\frac{(x_p - w_2)}{L_n} - \frac{\alpha L_n e^{\{\,-\alpha(x_p - w_2)\}}}{\cosh(\frac{x_p - w_2}{L_n})}\right] \tag{12}$$

and

$$\eta_{n^+}(\lambda) = \frac{\alpha L e^{-\alpha(x_n + x_p)}}{(\alpha^2 L^2 - 1)\cosh\frac{x_p}{L}}\left[\alpha L + \frac{e^{(-\alpha x_{p^+})} - \cosh(\frac{x_{p^+}}{L})}{\sinh(\frac{x_{p^+}}{L})}\right] \tag{13}$$

where D_n is the diffusion coefficient for electrons in the p-layer and L the diffusion length in the substrate. The quantum efficiency $\eta_w(\lambda)$ in the depletion region is

$$\eta_w(\lambda)=e^{-\alpha(x_n-w_1)}[1-e^{(-\alpha w_1)}]+e^{-\alpha x_n}[1-e^{(-\alpha w_2)}]. \tag{14}$$

The quantum efficiency $\eta_w(\lambda)$ depends on the width $W(=w_1+w_2)$ of the depletion region which is given by

$$W=\left[\frac{2\epsilon V_0}{q}\left(\frac{1}{N_a}+\frac{1}{N_d}\right)\right]^{1/2} \tag{15}$$

where ϵ is the dielectric constant of SiC, V_o the contact voltage of the n^+/p junction, and N_a and N_d the acceptor and the donor concentrations, respectively. Thus, we can obtain the total quantum efficiency $\eta_{total}(\lambda)$ as

$$\eta_{total}(\lambda)=\eta_p(\lambda)+\eta_n(\lambda)+\eta_{n^+}(\lambda)+\eta_w(\lambda). \tag{16}$$

The external quantum efficiency $\eta_{ext}(\lambda)$ is obtained by correcting $\eta_{total}(\lambda)$ for the reflection of light from the surface layer of the photodiode and is given by

$$\eta(\lambda)_{ext}=\eta_{total}(\lambda)[1-R(\lambda)]. \tag{17}$$

In addition, the quantum efficiency varies with the transmission of light through the SiO_2 layer overlying the n^+/p junction. The total transmittance $[1-R(\lambda)]$ of the incident light for an anti-reflective surface with a monolayer thickness of d is given by [5]

$$[1-R(\lambda)] =4n_on_s[n_o^2(1+n_s)^2-(1-n_o^2)(n_o^2-n_s^2)\sin^2\{g(\lambda)/2\}]^{-1} \tag{18}$$

where $g(\lambda)$ is the phase thickness of the optical coating, and n_o and n_s the refractive indices of the overlying SiO_2 layer and the underlying 4H-SiC layer, respectively. The phase thickness is given by

$$g(\lambda)=\frac{2\pi n_o d}{\lambda} \tag{19}$$

where d is the thickness of the anti-reflective layer. The minimum value of the reflectivity can be obtained when $g(\lambda)$ is π, 3π , ... $(2m-1)\ \pi$, (m is a positive integer).

III. CALCULATION OF THE QUANTUM EFFICIENCY

The parameters of the photodiode are required for the calculation of the quantum efficiency. They are the optical absorption coefficients as a function of wavelength, the mobilities and the diffusion lengths as functions of the increasing doping concentrations of each layer, the geometric structure of the photodiode, and the thickness of the anti-reflective layer. We used the optical absorption coefficients of 4H-SiC materials measured in the wavelength range of 200 $\sim$ 450 nm [8]. Our arguments were based on lifetimes of 20 ns and 10 ns for the electrons and the holes, respectively [2,9]. The diffusion lengths were determined by the definition relation between the carrier lifetime and the mobility and are listed in Table 1.

The quantum efficiency of the 6H-SiC photodiode was calculated by applying our diffusion model of the minority carriers in the n^+/p junction. Figure 2 shows the quantum efficiencies of the 6H-SiC photodiode calculated by using the parameters for device #1 listed in Table 2, together with those measured experimentally [2]. Because the calculated quantum efficiency nearly agreed with the measured one, as shown in Fig. 2, this model could be applied to calculate the quantum efficiency of the 4H-SiC photodiode.

The quantum efficiency contribution of each layer was calculated by using the parameters of device #2 given in Table 2. The curves of the individual contributions, together with the total quantum efficiency, are shown in Fig. 3 as a function of the wavelength λ . The contribution ratios to the total quantum efficiency were calculated by

$$\text{The contribution ratio}(\%)=\frac{\text{The integrated quantum efficiency of the layer}}{\text{The integrated total quantum efficiency}}\times 100. \tag{20}$$

The contribution ratios of the n^+-layer, the p-layer, the substrate, and the depletion region are 12.8, 46.2, 2.6, and 38.4% over the entire wavelength range between 200 nm and 380 nm, respectively; the contributions of the p-layer and the depletion region are very high. In addition, the contribution ratio of the n^+-layer is high at short UV wavelengths.

We calculated the quantum efficiency by varing the parameters in the p-layer for which the contribution ratio is very high. If the lifetime of the electrons in the p-layer increases, the quantum efficiency increases. Figure 4 shows the quantum efficiency calculated for different electron lifetimes, 50, 20, and 10 ns, in the p-layer and using the other parameters of device #2. The corresponding diffusion lengths were 3.6, 2.3, and 0.5 μm, respectively, keeping the electron mobility as 100 cm^2/Vs. By com-

paring (a) with (b) in Fig. 4, the maximum difference of the quantum efficiencies comes to about 10% at 270 nm. The quantum efficiency was calculated for different thicknesses of the p-layer by using the parameters of device #2. However, the quantum-efficiency curves did not change very much over the p-layer thickness range of 1 $\sim$ 5 μm.

Figure 5 shows the quantum-efficiency curves for three acceptor concentrations in the p-layer, as obtained by using the other parameters for device #2. If the acceptor concentration is decreased, lowering the p-doping level makes the electron mobility larger and the depletion region wider due to the high contact voltage of the n^+/p junction, as seen in Eq. (15). In addition, the contribution of the depletion region to the total quantum efficiency is increased by extending the depletion width; then, the contribution ratios are 63.2, 38.4, and 18.9% for the acceptor concentrations (a) 5.0×10^{15} cm^{-3}, (b) 5.0×10^{16} cm^{-3}, and (c) 5.0×10^{17} cm^{-3} in the p-layer, respectively. For these three doping levels of the p-layer and the parameters of device #2, the difference between quantum efficiencies (a) and (b) in Fig. 5 comes to about 20% at 270 nm.

Figure 6 shows the quantum-efficiency curves for different thicknesses of the n^+-layer, as obtained by using the other parameters of device #2. As the n^+-layer thickness is decreased from 0.2 μm to 0.05 μm, the quantum efficiency is significantly increased at shorter UV wavelengths. The peak of the quantum efficiency is shifted toward shorter UV wavelength as shown in Fig. 6 because the optical absorption of shorter wavelengths is very high near the surface of the n^+-layer. An extremely thin n^+-layer is required to enhance the collection efficiency in the shorter UV range [12]. If the n^+-layer thickness is below 0.2 μm in device #2, the quantum-efficiency peak can be increased to above 78% at 257 nm, and the difference of the quantum efficiency between (a) and (b) in Fig. 6 will come to about 15% at a wavelength of 257 nm.

IV. RESULTS AND DISCUSSION

In order to obtain higher quantum efficiencies, a shallow n^+/p junction, a highly doped n^+-layer and lowly doped p-layer, large values of the mobilities and the lifetimes of the minority carriers in the n^+- and the p-layers are required. The photoresponse mostly depends on the surface recombination velocity and the lifetime in the top region. The surface recombination velocity in the n^+-layer must be estimated for the calculation of the quantum efficiency of the photodiode. Figure 7 shows the quantum-efficiency curves of the photodiode which are calculated for different surface recombination velocities in the n^+-layer by using the parameters of device #2. The quantum efficiency decreases with increasing surface recombination velocity in the shorter UV range. By assuming that the surface of the n^+-layer contained a large number of recombination centers [2], the surface recombination velocity of the 6H-SiC photodiode was estimated to be above 3.0×10^7 cm/s which is very high. This surface recombination velocity was used for our calculation of the quantum efficiency. The quantum efficiency increased in the shorter wavelength range of 200$\sim$250 nm as the surface recombination velocity decreased.

A heavily doped n^+-layer is useful for obtaining a wider depletion region in the n^+/p junction, which makes the quantum efficiency contribution of the depletion region higher, as shown by Eq. (14). Therefore, the contribution of the depletion region should be considered whenever the quantum efficiency is calculated. The donor concentration of the n^+-layer was chosen to be 5×10^{18} cm^{-3}, which is high. An increase of the donor concentration in the n^+-layer should lead to an improvement of the collection efficiency after a reduction of the n^+-layer thickness; an improvement due to the simultaneously decreased series resistance will also occur. As a thin n^+-layer makes the depth of the n^+/p junction shallow, the quantum efficiency is increased in the short wavelength range below 250 nm as seen in Fig. 6. The thickness of the n^+-layer was chosen to be about 0.05 μm.

As the doping in the n^+-layer increases, the depletion region extends toward the p-layer side. Accordingly, the parameters in the p-layer are important. A large value of the diffusion length in the p-layer, as well as a low level of doping in the p-layer, is effective for obtaining a higher collection efficiency, as mentioned above. The acceptor concentration of the p-layer was estimated to be 5×10^{15} cm^{-3}, which is low. Moreover, a long lifetime for the electrons in the p-layer is very effective for increasing the quantum efficiency in the wavelength range of 250 $\sim$ 320 nm, as shown in Fig. 4.

Now, we can choose the device parameters of the 4H-SiC photodiode so as to obtain higher quantum efficiency. The above arguments lead to a high electron mobility and a long lifetime in the p-layer, a lower acceptor concentration in the p-layer, a higher donor concentration in the n^+-layer, and a thin n^+-layer. Figure 8 shows the internal quantum efficiency calculated by using the parameters for device #4, except the SiO_2 layer, which were chosen to enhance the quantum efficiency in the UV range. We expected the 4H-SiC photodiode to show a good photoresponse in the wavelength range between 200 nm and 380 nm. The contribution ratio for the depletion region was very high, about 70%. The peak value of the total internal quantum efficiency came to about 92% at 257 nm.

Finally, we compare the external quantum efficiency of the 4H-SiC photodiode with those of a 6H-SiC photodiode. As seen in Fig. 9, the calculated quantum efficiency (c) of the 4H-SiC photodiode (device #4) is higher than both the calculated one (b) of 6H-SiC (device #3 with nearly same parameters) in the shorter UV range and the measured one (a) (device #1 with another parameters).

The peak of the external quantum efficiency of the 4H-SiC photodiode (about 90% at 257 nm) (device #4) is higher by about 5% than that of the 6H-SiC photodiode (about 85% at 270 nm) (device #3).

As seen in Fig. 9, the quantum-efficiency curve of the 4H-SiC photodiode, compared with that of 6H-SiC photodiode, is shifted toward the shorter UV wavelength because the bandgap of 4H-SiC (3.26 eV at 300 K) is larger than that of 6H-SiC (2.93 eV at 300 K). Accordingly, the optical absorption edge of 4H-SiC (380 nm) is shorter than that of the 6H-SiC (417 nm). The optical absorption coefficients can be increased by increasing the doping carrier concentration. However, even if the optical absorption coefficients are increased by about 10%, the difference in the quantum efficiency is below 3% between 250 nm and 300 nm.

The electron and the hole mobilities of 4H-SiC are higher than those of 6H-SiC in the [0001] direction for the same carrier concentration because of the smaller effective mass of 4H-SiC (see Table 3). As the mobility is increased, the diffusion length (L) is lengthened by the relation between the diffusion length L and the diffusion coefficient D ($L \equiv \sqrt{D\tau}$). The longer diffusion length of 4H-SiC increases the quantum efficiency, as calculated in Eq. (16), so the quantum efficiency of the 4H-SiC photodiode is higher than that of the 6H-SiC photodiode at shorter UV wavelengths. Accordingly, the higher mobility of 4H-SiC must be considered as a main parameter in increasing the quantum efficiency. We expect the photoresponse of the 4H-SiC photodiode to be superior to that of the 6H-SiC photodiode at shorter wavelength because the higher mobilities of 4H-SiC make the diffusion length longer.

A SiO_2 layer on the surface of the n^+/p junction is considered as an anti-reflective layer to improve the quantum efficiency. The refractive index of SiO_2 should equal the square root of the index of the underlying SiC layer for zero reflectance on the front surface of the photodiode. Even though the refractive indices of the SiO_2 and the SiC layers used to show the effect of anti-reflection do not satisfy the square-root condition ($n_0 = \sqrt{n_s}$) of complete transmission, the maximum transmittance is very high, about 98%. Owing to the oscillation period of the transmittance, we can adjust the thickness of the anti-refractive SiO_2 layer in order to obtain the optimal quantum efficiency at the required wavelength. Figure 10 shows the refractive index of 4H-SiC as measured in the wavelength range of 250 $\sim$ 500 nm by the ellipsometry. The external quantum efficiency for different thicknesses of the SiO_2 layer was calculated using the refractive index of 4H-SiC.

Figure 11 shows the effect of the anti-reflective SiO_2 with a thickness of 572 nm ($m = 5$, in Eq. (19)) using the other parameters of device #4 as an example. The refractive index in the wavelength range of 200 $\sim$ 250 nm was extrapolated for the calculation of the quantum efficiency. The SiO_2 thicknesses are well matched with the SiC layer to get maximum transmittance for Argon-laser light of 257-nm. As seen in Fig. 11, the oscillation period of the transmittance gradually decreases with increasing SiO_2 thickness relative to the phase condition of Eq. (19).

V. CONCLUSIONS

We have calculated the quantum efficiency of an UV photodiode using 4H-SiC. For higher collection efficiency, we considered a very thin n^+-layer, and high and low doping in the n^+-layer and the p-layer, respectively. Our arguments are based on carrier lifetimes of 20 ns and 10 ns for electrons and holes, respectively. The parameters were properly chosen to increase the quantum efficiency and to optimize it at UV wavelength. We calculated the quantum efficiency for various parameters to select their optimal values. The calculated quantum efficiency was compared with those of the measured and the calculated one for a 6H-SiC UV photodiode. The contributions of the quantum efficiency from the p-layer and the depletion region are considerable in the wavelength range between 200 nm and 300 nm.

We expect a good photoresponse in the 4H-SiC homostructure for the wavelength range of 200 $\sim$ 380 nm. The highest internal quantum efficiency of a 4H-SiC photodiode came to about 92% with a peak at 257 nm. In the shorter UV range, the peak of the external quantum efficiency of a 4H-SiC photodiode (about 90% at 257 nm) (device #4) was higher by about 5% than that of a 6H-SiC photodiode (about 85% at 270 nm) (device #3) with nearly the same parameters. The peak of the quantum efficiency of the 4H-SiC photodiode compared with that of the 6H-SiC photodiode was shifted toward shorter UV wavelength.

REFERENCES

[1] J. W. Palmour, J. A. Edmond, H. S. Kong and C. H. Carter, Physica B**185**, 461 (1993).
[2] D. M. Brown, E. T. Downey, M. Ghezzo, J. W. Kretchmer, R. J. Saia, Y. S. Liu, J. A. Edmond, G. Gati, J. M. Pimbly and W. E. Schneider, IEEE Trans. on Electron Devices **40**, 325 (1993).
[3] A. Itoh, H. Akita, T. Kimoto and H. Matsunami, Appl. Phys. Lett. **65**, 1400 (1994).
[4] R. Van Overstraeten and W. Nuyts, IEEE Trans. on Electron Devices ED-**16**, 632 (1969).
[5] H. J. Hovel, *Semiconductors and Semimetals* 11 (Academic Press, New York, 1975), p. 203.
[6] K. S. Park and K. A. Lee, J. Korean Phys. Soc. **29**, 225 (1996).
[7] S. M. Sze, *Physics of Semiconductor Devices* (John Wiely Sons, New York, 1981), p. 800.
[8] H. R. Philip, Phys. Rev. **111**, 440 (1958).
[9] P. Glasow, G. Ziegler, W. Suttrop, G. Pensl and R. Heibeg, SPIE **868**, 40 (1987).

[10] W. J. Schaffer, H. S. Kong, G. H. Negley and J. W. Palmour, *The 5th SiC and Related Materials Conf.* 137 (1993).
[11] G. G. Harman and R. L. Raybold, Appl. Phys. **32**, 1168 (1961).
[12] H. Ouchi, T. Mukai, T. Kamei and M. Okamura, IEEE Trans. on Electron Devices ED-**26**, 1965 (1979).
[13] D. L. Barret and R. B. Campbell, J. Appl. Phys. **38**, 53 (1967).
[14] D. R. Hamilton, L. Patrick and W. J. Choyke, Phys. Rev. **138**, 1742 (1965).
[15] W. Götz, A. Schöner, G. Pensl, W. Suttrop, W. J. Choyke, R. Stein and S. Leibenzeder, J. Appl. Phys. **38**, 53 (1967).
[16] A. Itoh, *Control of Electrical Properties of 4H-SiC Grown by Vapor Phase Epitaxy for Power Electronic Application* (Thesis of Doctor Degree, Kyoto University, Kyoto, 1995), p. 11.